www.elsevier.com/locate/memsci

Study of different titanosilicate (TS-1 and ETS-10) as fillers for Mixed Matrix Membranes for CO_2/CH_4 gas separation applications

V. Martin-Gil, A. López, P. Hrabanek, R. Mallada, I.F.J. Vankelecom, V. Fila

PII: S0376-7388(16)31737-9
DOI: http://dx.doi.org/10.1016/j.memsci.2016.09.041
Reference: MEMSCI14762

To appear in: *Journal of Membrane Science*

Received date: 15 December 2015
Revised date: 20 September 2016
Accepted date: 24 September 2016

Cite this article as: V. Martin-Gil, A. López, P. Hrabanek, R. Mallada, I.F.J. Vankelecom and V. Fila, Study of different titanosilicate (TS-1 and ETS-10) as fillers for Mixed Matrix Membranes for CO_2/CH_4 gas separation applications *Journal of Membrane Science,* http://dx.doi.org/10.1016/j.memsci.2016.09.041

Study of different titanosilicate (TS-1 and ETS-10) as fillers for Mixed Matrix Membranes for CO_2/CH_4 gas separation applications.

V. Martin-Gil[1,4], A. López[2], P. Hrabanek[3], R. Mallada[2], I.F.J. Vankelecom[4], V. Fila[1]

[1]Department of Inorganic Technology, University of Chemistry and Technology, Prague, 16628, Czech Republic.

[2]Department of Chemical Engineering, Nanoscience Institute of Aragon (INA), Universidad de Zaragoza, E-50018-Zaragoza, Spain.

[3]Heyrovský Institute of Physical Chemistry of the ASCR, v.v.i.; Dolejškova 2155/3, 18223 Prague 8, Czech Republic

[4]Centre for Surface Chemistry and Catalysis, KU Leuven, Kasteelpark Arenberg 23, 3001 Heverlee, Belgium

Abstract

Three titanosilicate zeolites were used as fillers for Mixed Matrix Membranes: (i) ETS-10, (ii) TS-1 having Si/Ti = 100 and (iii) TS-1 using Si/Ti = 25. Zeolite samples were characterized by X-Ray Diffraction, Scanning Electron Microscopy, Atomic Emission Spectroscopy, X-Ray Photoelectron Spectroscopy, and CO_2 and CH_4 adsorption isotherms. TS-1 particles showed a narrow size distribution ranging from 200 nm to 400 nm. In the case of ETS-10, the size distribution was broader ranging from 400 nm to 800 nm. Mixed Matrix Membranes were prepared using Matrimid® polyimide as continuous phase and filler loadings of 10, 20, and 30 wt.%. Membranes were characterized by Thermogravimetric Analysis, Differential Scanning Calorimetry, and Scanning Electron Microscopy. The performances was measured at 8 bars of transmembrane pressure for CO_2/CH_4 mixed gases system at 50/50 vol./vol. concentration.

Membranes using TS-1 (Si/Ti = 25) as filler showed a maximum increase of 89.1% of CO_2 permeability and 23.9% increase in separation factor. In the case of TS-1 (Si/Ti = 100) only permeability increased significantly, with a maximum increase of 90.1%. Regarding the ETS-10 membranes, both permeability and separation factor increased slightly with respect to the reference polymeric membrane (22.5% in CO_2 permeability and 7.8% in the separation factor). In conclusion, TS-1 (Si/Ti = 25) is the most suitable filler for the use in Mixed Matrix Membranes for gas separation applications among the titanosilicate studied in this work.

Keywords: Titanosilicate, Mixed Matrix Membrane, CO_2/CH_4 separation, TS-1, ETS-10

1. Introduction

In 2012, world consumption of natural gas was around 3400 billion of (STP)m^3 [1], and since then it has been increasing year by year. Natural gas is one of the most common raw materials not only for power supply but also for chemical industry, so purification of these gases by means of membrane technologies is becoming a challenge for researchers. Currently, the most used techniques are based on absorption of acid gases in basic solvents which brings the need of solvent regeneration, difficult application for small gas fields and lack of robustness against fluctuations of feed composition [2]. Deterioration of the quality of natural gas sources is a fact that must to be taken into account for future exploitations of this natural resource. Natural gas separation using membrane technologies is one of the most promising applications due to the fact that this technology is able to reduce not only operating costs and energy requirements, but also offers easy operating and low capital costs [3]. Therefore, removal of carbon dioxide from methane using membrane technologies is an extraordinary application in which the worldwide market for new purification equipment may exceed $5 billion per year [4]. Moreover, there are many other applications where membrane technology shows potential to become an alternative to the traditional processes, such as air separation, hydrogen or hydrocarbons recovery, helium separation and recovery or CO_2 sequestration to reduce greenhouse gas emissions [5]. In the case of CO_2 removal from CH_4, there are other applications apart of natural gas separation, such as biogas upgrading or oil recovery enhancement [6].

Research is still required to improve the separation performance of membranes and increase the time-life of membranes [6]. In 1991, Robeson [7] did a statistical analysis for many different polymer materials and different pairs of gases and found a trade-off in which an upper bound limit is established. This trade-off says that when permeability increases, selectivity decreases and vice versa. In 2008, this upper bound was revised and new limits for each pair of gases were established [8].

Mixed Matrix Membranes (MMMs) have caught the attention of many researchers in last few years [9–12] in order to improve gas separation performance of polymeric membranes and achieve the necessary features for industrial applications. Introduction of inorganic fillers has emerged as a potential approach to overcome limitations of ceramic and polymeric membranes. Although silica particles have been widely studied [13–17], only a few studies using titanosilicate have been done for gas separation processes. For instance, Galve et al. studied MMM using microporous layered titanosilicate JDF-L1 [18,19]. Nevertheless, it is worthy to note that final features of MMMs are not as simple as the mixture of properties of both materials. Complex changes in the structure of polymer and filler surfaces are formed. Using polyimides as continuous phase is becoming a widespread option for CO_2 selective applications. These polymers present outstanding features in terms of thermal and chemical stability, besides good mechanical properties, and high selectivities with good permeabilities [20,21]. Matrimid® is a commercial thermoplastic polyimide with excellent mechanical, thermal and chemical properties. In the Fig. 1, the chemical structure of Matrimid® is depicted.

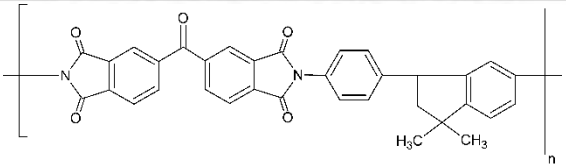

Fig. 1. Chemical structure of Matrimid®

Zeolite and zeolite-like (zeotype) materials with their unique tetrahedral framework structures and compositions, uniform pores, well-defined acidity, cation exchange selectivity, and good thermal stability are widely used as commercial catalysts, ion exchangers, and adsorbents [22]. Microporous titanosilicate zeolites have some advantages over more conventional aluminosilicate zeolites: i) they are normally prepared under mild pH conditions, reducing the chance corrosion of the synthesis set-up, ii) the combination of octahedral and tetrahedral oxides gives the opportunity of isomorphous framework substitution and therefore, the tuning of adsorption properties while preserving its microporous structure [23].

In the Fig. 2, the structure of Titanium silicate 1 (TS-1) can be seen. TS-1 zeolites belong to MFI framework zeolites. TS-1 are a crystalline zeotype material in which tetrahedral [TiO_4] and [SiO_4] units are arranged in an MFI structure. TS-1 was synthesized for the first time in 1986 by Tamarasso et al. [24]. Its structure can be described with pentasil units. These units are linked to form pentasil chains, and mirror images of these chains are connected via oxygen bridges to form corrugated sheets with 10-rings. Each sheet is linked by oxygen bridges to the next to form the 3-dimensional structure [25]. This 3D structure is a system of interconnected channels parallel to [100] and [010] directions with elliptical ten-ring apertures of 5.1×5.5 Å and 5.3×5.6 Å. It is based on ten oxygen ions per aperture with radii of 1.35 Å. There are four interconnections per unit cell, straight channels parallel to [010] connect in 90° angle with the sinusoidal channel along the [100] direction, in these intersections large cavities of 9 Å in diameter are created [26][27].

In previous works, Mirajkar et al. [28] investigated the influence of titanium content in the zeolite on the sorption properties of TS-1. They reached the conclusion that at higher content of Ti, higher was the sorption of the vapors studied: water, n-hexane, cyclohexane and n-butylamine. When there is more Ti incorporated into the silica matrix, the number of linkages Si-O-Ti also increases; hence the sorption capacity increases. They also observed that the incorporation of Ti (IV) species replacing Si (IV) increases the unit cell volume. In the work of Langerame et al. [29], it is explained that each Ti (IV) site of the framework chemisorbs two water molecules from atmosphere to adopt its preferential octahedral coordination. All these parameters can affect the performance of a MMM using TS-1 with different content of Ti.

ETS-10 (Engelhard Corporation titanosilicate) is a zeotype synthesized for the first time in 1989 by Kunicki et al. [30]. A more appropriate building block is taken as $Si_{40}Ti_8O^{-16}_{104}$ unit. It makes a charged framework. TiO_6 octahedral are linked to each other forming a straight chain. These chains are parallel to the orthogonal channels and alternate in direction along the c-axis during the stacking. Rods composed by a titanium chain surrounded on both side by silicon five-rings are connected perpendicularly and generate seven-rings. As a result of the complete stacking of these rods, large 12-rings (7.6 × 4.9 Å) are encompassed [31]. ETS-10 structure is displayed in the Fig. 2.

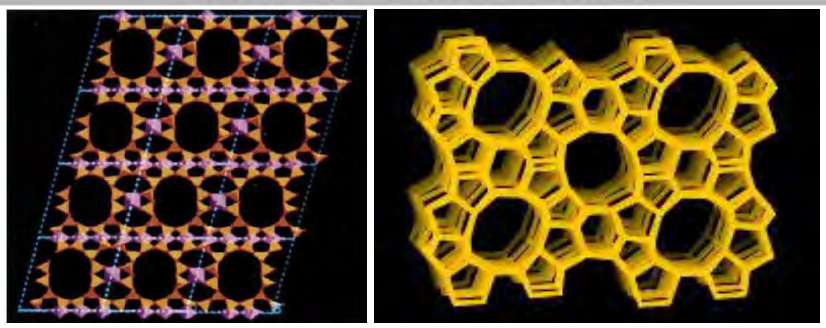

Fig. 2. A) Projection down the [110] axis of ETS-10 structure [31]*and B) Projection along [010] of MFI zeolite [32]. *Reprinted by permission from Macmillan Publishers Ltd: Nature (367, 347-351), copyright 1994.

The synthesis of small crystals of ETS-10 is important to get high-quality titanosilicate ETS-10 membranes prepared with a good degree of crystal intergrowth and gas separation properties [33]. Changing the titanium source could lead to ETS-10 particles with different size. The smallest crystal sizes were obtained using TiO_2-anatase while $TiCl_3$ yielded the largest sizes [34]. Furthermore, it has been reported previously in the literature that ETS-10 is a basic material and can adsorb CO_2 at low temperature, this property makes that ETS-10 membranes can separate CO_2 from binary mixtures of CO_2/N_2 and CO_2/H_2 by preferential adsorption and diffusion of CO_2 [35]. Anson et al. [36] studied the adsorption capacity of ETS-10 and ETS-4 for carbon dioxide, methane and ethane. These zeolite showed high theoretical limiting selectivity based on Henry's constant for CO_2/CH_4 ($\alpha_{ETS\text{-}10}$ = 320 and $\alpha_{ETS\text{-}4}$ = 350).

In our work, we choose TS-1 with different content of titanium in the zeolite as filler for MMMs in order to check the influence of Ti on the performance of the different MMMs. In the other hand, ETS-10 has been chosen by its high limiting selectivity and the small particle size obtained for this work (around 650 nm).

2. Experimental

2.1. Materials

Polymer used as continuous phase was commercial polyimide Matrimid® 5218 supplied by Huntsman. It is a completed imidized thermoplastic polyimide with a molecular weight of 44000 g/mol [37]. Germany. N-methyl-2-pyrrolidinone, NMP (99% extra pure) from Sigma Aldrich was chosen as solvent.

For the synthesis of TS-1, used reactants were: titanium (IV) n-butoxide 99% (TBOT) purchased from Acros Organist as titanium source, tetraethoxysilane 99.9% (TEOS) from Alfa Aesar as silicon source, and tetrapropylammonium hydroxide (TPAOH) solution (~20% wt. in water) from Fluka Analytical as template. Moreover, 2-propanol 99.9% from Fluka Analytical was used as solvent.

The ETS-10 particles were synthesized using sodium chloride (Merck, 99% purity), potassium chloride (Merck, pro-analysis grade), sodium silicate (Merck, 25.5-28.5% SiO_2 and 7.5-8.5% Na_2O), potassium fluoride (Aldrich, 99% purity), titanium dioxide (anatase, Aldrich, 99.8% purity). All chemicals were used as received.

2.2. TS-1 synthesis

TS-1 zeolites were prepared by hydrothermal synthesis. Mother solution used to synthesize TS-1 particles was obtained by mixing two individually prepared solutions. Solution A (the silica source) was prepared by mixing desired amount of TEOS and TPAOH, while solution B (titanium source) was prepared by mixing TBOT and 2-propanol. These two solutions were then mixed rapidly. After addition of water to bring solution to the balance, it was stirring for 6-7 h at 65 °C in order to complete the hydrolysis. The final molar ratio of the solution is x TiO_2: 1 SiO_2: 0.18 TPAOH: 75 H_2O. After hydrolysis, the solution was aged for 7 days at 40 °C. The solution was then transferred into a Teflon® linen autoclave for hydrothermal synthesis at crystallization temperature of 140 °C for 24 h. To separate the particles after synthesis, the solution was centrifuged and washed with deionized water three times. TS-1 particles were dried at 120 °C overnight. Template removal was carried out at 480 °C for 24 h with a heating and a cooling rate of 0.5 °C/min. This step of the synthesis was carried under a nitrogen flow of 50 ml/min. Two different Si/Ti are used to synthesize these particles, Si/Ti = 100 and Si/Ti = 25, obtained particles are named TS-1-100 and TS-1-25 respectively.

2.3. ETS-10 synthesis

ETS-10 particles were synthesized by means of hydrothermal synthesis method to prepare a gel of molar composition 4.4 Na_2O: 1.4 K_2O: TiO_2: 5.5 SiO_5: 125 H_2O. In a typical synthesis an aqueous solution consisted of 5.06 g of NaCl, 1.23 g of KCl and 23.22 g of deionized water was prepared. After that, 17.69 g of sodium silicate were added drop by drop avoiding to form a solid gel by means of increasing the stirring solution. This solution was vigorously stirred for 3 h in order to obtain a homogenous gel. 1.57 g of KF as potassium source were added and stirred till it was dissolved. Finally 1.22 g of TiO_2 were added and stirred for 1 h to obtain a milky homogenous gel of pH = 10.4. Gel was transferred to a Teflon® linen autoclave, placed inside the oven at 230 °C and maintained at this temperature for 24 h. Obtained product was washed and centrifuged at 8000 rpm for 20 min until the discarded water had a pH between 9 and 10.

2.4. Membrane preparation

2.4.1. Pure Matrimid -PI membrane

Membranes were prepared by solvent evaporation. Matrimid® 5218 powder was dried at 100 °C under vacuum overnight. A 10 wt.% solution was prepared using NMP as solvent. Dope solution was prepared by adding a third part of the total amount of polymer and stirring it for 2 h. Other third of the total polymer was added and mechanically stirred for 2 h. It was repeated once more to add the whole amount of polymer. Then, the dope solution was stirred for 24 h and sonicated for 1 h. Finally, the dope solution was cast on a flat glass plate using a 0.47 mm casting knife. Solvent was allowed to evaporate in a nitrogen box for 4 days. Obtained film was detached by water and dried for 24 h at 120 °C.

2.4.2. Mixed Matrix Membranes (MMM)

MMM samples were prepared similarly. Firstly, a particle suspension was prepared in NMP; the required amount of each titanosilicate was added to NMP and sonicated for 15 min, stirred for 2 h, sonicated for 15 min again and then stirred overnight. Secondly, a third of the polymer was added and stirring for 2 h till it was dissolved and the dope solution was sonicated for 15 min. This procedure was repeated twice and the final

sonication was done for 1 h. Finally, the solution was cast onto a glass surface with a casting knife of 0.47 mm height and placed in a nitrogen box. Solvent was evaporated for 7 days. Samples were detached with water and dried at 120 °C for 24 h. All sample thicknesses were measured using a digital micrometer Mitutoyo with 1 μm resolution. Sample thicknesses ranged between 20 and 60 μm.

The necessary amount of zeolite for the different loadings was calculated using Eq. 1

$$\text{Zeolite loading (wt.\%)} = \left[\frac{\text{wt.Zeolite}}{\text{wt.Zeolite+wt.polymer}}\right] \cdot 100 \qquad \text{Eq. 1}$$

2.5. Characterization

Different titanosilicates were characterized by scanning electron microscopy (SEM) Hitachi S4700 in order to check the morphology of the particles. Particle size and particle size distribution was calculated by means of Imaq Vision Builder software using different SEM micrographies. Cross-sections of membranes were characterized using a Scanning Electron Microscope (SEM) JEOL-JSM-5600LV for investigating the compatibility of the different titanosilicates and the polymeric phase. Cross-sections were obtained by cryogenic fracture by immersion the samples in liquid nitrogen

Crystallinity of the samples was studied by XRD analyses. They were carried out using XRD-Diffractometer PANalytical X'Pert PRO (PANalytical Holland) using CuKα radiation with a voltage and current of 40 kV and 30 mA respectively.

Chemical composition of the particles was studied by Atomic Emission Spectroscopy (AES) in order to determine the real content of Ti and the actual Si/Ti. AES analyses were carried out using Perkin Elmer 8000 Optima ICP-OES – Inductively Coupled Plasma Optical Emission Spectroscopy. Samples were dissolved using an equal mixture in volume of HF: HNO_3: HCl using the protocol described previously in literature [38].

Chemical surface characterization of the zeolites was performance by X-Ray Photoelectron Spectroscopy (XPS). The X-ray photoelectron analysis (XPS) was performed with an Axis Ultra DLD (Kratos Tech.). The spectra were excited by a monochromatized AlKα source (1486.6 eV) run at 15 kV and 10 mA. The binding energies were referenced to the internal C1s (284.9 eV) standard.

Thermal properties of membranes were investigated by Thermal Gravimetric Analysis (TGA) and Differential Scanning Calorimetry (DSC) using a Linseis STA 700LT. Analyses were carried out using a sample between 4 and 7 mg placed in an alumina crucible. Simultaneous TGA and DSC analyses were carried out heating up the sample to 700 °C with a heating rate of 20 °C/min. under nitrogen flow of 20 ml/min. Temperature was hold at 700 °C for 30 min and then cooled down to 50 °C at 20 °C/min. Glass transition temperature (T_g) was determined by DSC tests using the inflexion point in the step of specific heat curve.

2.6. Gas separation evaluation

Gas separation measurements were carried out in high throughput gas separation (HTGS) equipment [39]. Measurements were performed using mixed gas feed composed by 50/50 vol./vol CO_2/CH_4 under 8 bar feed pressure at 35 °C. HTGS system was evacuated for 1 h and then feed stream was applied for 2 h before starting of measurements in order to

reach the steady state of the membranes. Permeabilities were measured under constant-volume/variable-pressure principle using Eq. 2 and Eq. 3 [40] where y_i and x_i are the molar fraction in the permeate and feed stream respectively, V_d is the calibrated permeate volume in cm^3, l is the thickness of the membrane in cm, ΔP is the pressure difference between the applied feed pressure and downstream pressure in cmHg, A is the effective area of the membrane in cm^2, R is the ideal gas constant (0.278 cm^3·cmHg/(cm^3(STP)K), and T is the operation temperature in K.

$$P_{CO_2} = \frac{y_{CO_2} V_d l}{x_{CO_2} \Delta P A R T} \frac{dP}{dt} \quad \text{Eq. 2}$$

$$P_{CH_4} = \frac{y_{CH_4} V_d l}{x_{CH_4} \Delta P A R T} \frac{dP}{dt} \quad \text{Eq. 3}$$

Selectivity was determined through the composition of the permeate stream via a compact gas chromatograph (CGC, Interscience, Belgium) using Helium as carrier gas and thermal conductivity detector (TCD). Selectivity values were calculated through Eq. 4 where x_i and y_i are the molar fractions in the feed and permeate stream respectively.

$$\alpha_{CO_2/CH_4} = \frac{y_{CO_2}/y_{CH_4}}{x_{CO_2}/x_{CH_4}} \quad \text{Eq. 4}$$

In order to compare the results easily and observe more clearly the influence of the different zeolite loading on the gas separation performance, the normalized permeabilities and selectivities are presented too. Normalized permeabilities and selectivities were calculated using Eq. 5, Eq. 6 and Eq. 7.

$$P_{Normalized}(CO_2) = \frac{\overline{P_{CO_2}}(MMM)}{\overline{P_{CO_2}}(Matrimid)} \quad \text{Eq. 5}$$

$$P_{Normalized}(CH_4) = \frac{\overline{P_{CH_4}}(MMM)}{\overline{P_{CH_4}}(Matrimid)} \quad \text{Eq. 6}$$

$$Sep.\,Factor_{Normalized} = \frac{\overline{Sep.Factor}(MMM)}{\overline{Sep.Factor}(Matrimid)} \quad \text{Eq. 7}$$

3. Results and discussion

3.1. Zeolite Characterization

3.1.1. XRD

In Fig. 3A, the XRD patterns for as-synthesized TS-1 particles can be observed. Characteristic peaks for TS-1 at (2θ= 7.9°, 8.8°, 23.1°, 23.9°) representatives of MFI structure can be seen. These peaks correspond to the d-spacing 11.2, 10.1, 3.8, and 3.7 Å, and to the directions ⟨011⟩ ⟨020⟩ ⟨051⟩ and ⟨511⟩ respectively [41]. Moreover, no peaks are detected at 2θ= 25.3°, 37.9°, 48.4°; which would disclose the existence of anatase TiO_2 phase [42]. Therefore, the synthesis procedure was successful in both cases and titanium cations are included into the framework of the zeolite. Furthermore, the peak at 29.2° corresponding to d-spacing 3.05 Å and the direction of ⟨352⟩ is an appropriate evidence of the incorporation of Ti into the framework [41]. In Fig. 3B, XRD pattern of ETS-10 is shown, diffractogram presents peaks that are in agreement with those published by other

authors for ETS-10 [34,43,44]. Besides, the purity and crystallinity of ETS-10 obtained was analyzed. It is also noted that there are no remains of the synthesis gel. On the other hand, the pattern of the solid prepared presents a peak related to quartz impurity [34] (labeled with an x), this was previously reported when using anatase as Ti source and a similar gel composition [45].

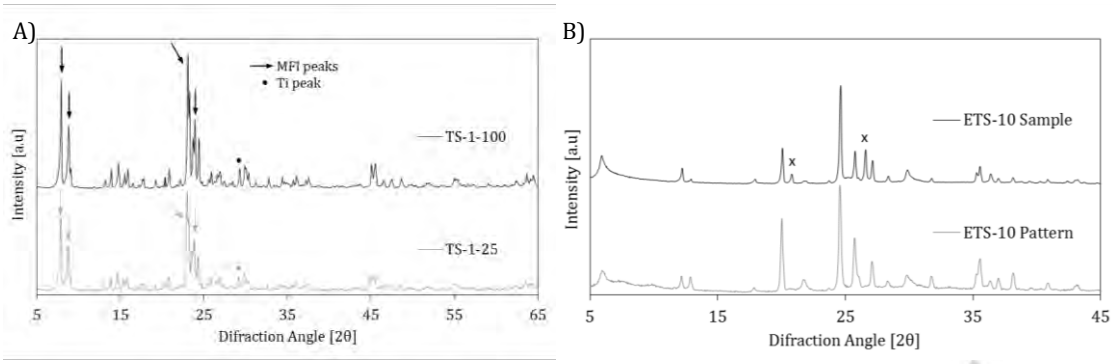

Fig. 3. XRD Patterns of A) TS-1-25 and TS-1-100 and B) ETS-10.

3.1.2. SEM

Fig. 4 shows the SEM images of as-synthesized TS-1 and ETS-10 particles. Regardless the morphology of the TS-1 particles, SEM images show that all particles present an orthogonal shape and a narrow size distribution. The histograms show that the TS-1-100 follow a normal distribution centered at around 260 nm, the average particle size (N = 50) is 257 ± 25 nm. TS-1-25 particles show a mean particle size (N = 50) of 419 ± 30 nm and do not follow a normal distribution, exhibiting a broad range in particle size ranging from 350 to 475 nm. The ETS-10 particles show a rhombohedral morphology and their size is 610 ± 67 nm. ETS-10 particles show the broadest distribution (N = 50) which ranges from 450 to 800 nm. The size of the particles synthesized in this work is in agreement with other small particle size reported in literature such as the results of the work of Faroldi et al. [46] where a ETS-10 the particle size reported is 400 - 600 nm. Casado et al. [34] reported a particle size of 320 x 410 nm. Lv et al. [45] reported bipyramidal particles of 500 nm. Histograms of the different particle size distribution can be observed in Fig. S1 of ESI.

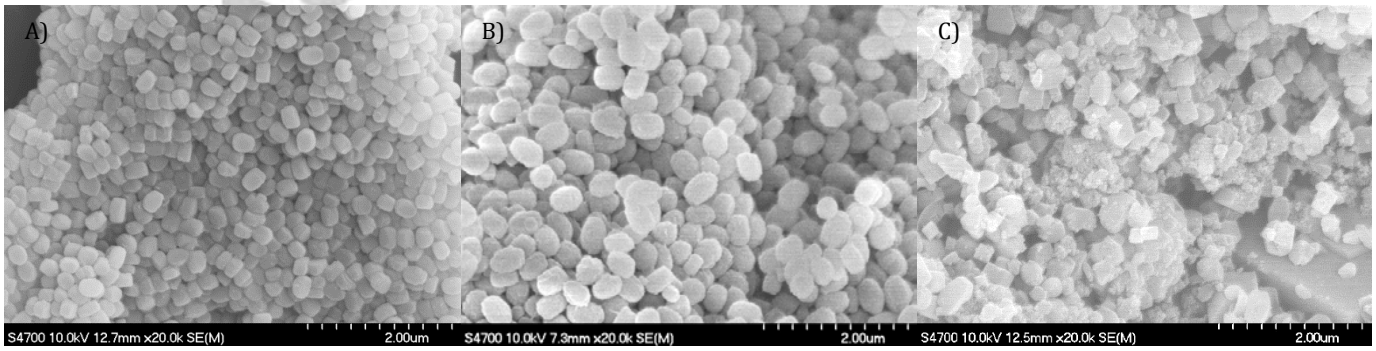

Fig. 4. SEM images of nanoparticles A) TS-1-100, B) TS-1-25 and C) ETS-10.

3.1.3. Chemical Characterization

Table 1 shows the results obtained by AES-ICP and XPS analyses. AES-ICP results show the actual content of Ti in the zeolites, besides the real value Si/Ti. Regarding TS-1-100, actual Si/Ti is very close to the theoretical one. However TS-1-25 shows a lower Si/Ti than the ratio of the mother solution. The maximum content of Ti in TS-1 corresponds to ca 2.4 atoms of Ti per unit cell which leads to a maximum Ti content of 1.98 wt.% [29] incorporated in the zeolite framework. For this reason the incorporation of Ti in the zeolite framework is limited. On the other hand, ETS-10 incorporates more Ti due to its different structure. Comparing Si/Ti in the bulk with Si/Ti in the surface, a large difference is found in the three zeolites. The higher content of Ti on the surface than in the bulk of the zeolite can be due to the segregation of TiO_2 species (<5 nm) during the synthesis [47].

Regarding XPS analyses (spectra are depicted in Fig S2 of ESI), peaks at different binding energy (BE) are related to the different oxidation states and coordination of Ti in the zeolite. The peak at 457 eV is assigned to Ti (III), the peaks at higher BE are assigned to Ti (IV), either in octahedral coordination as for pure TiO_2, (peak 2 at 458,5 ev) or Ti (IV) in tetrahedral coordination (peak 3 at 460 eV) [29]. Table 1 summarizes the XPS results after deconvolution of the peaks. Concerning ETS-10, all Ti is coordinated in octahedral position. The difference between Si/Ti in the bulk and Si/Ti in the surface suggests that part of Ti was segregated in form of TiO_2 in the surface of the particles. Regarding TS-1, differences on the surface composition are found. A higher percentage of octahedral Ti is observed in TS-1-25 than in TS-1-100 which is related to the higher formation of TiO_2 nanoparticles on the surface. The other main difference on the surface composition between the TS-1-100 and TS-1-25 is the percentage of Ti (III) related to peak 1. This difference can be due to the higher segregation of TiO_2 which would cover the Ti (III) placed in a deeper position non detectable by XPS.

Table 1. Surface and bulk chemical composition of titanosilicates. [a]Data determined by AES-ICP analyses and [b]data obtained by XPS analyes

	Si/Ti[a] (bulk)	**Ti content[a] [wt. %]**	**Si/Ti[b] (Surface)**	**BE Ti 2p 3/2[b] [atomic %]**		
				Peak 1 457 [eV]	**Peak 2 458.5 [eV]**	**Peak 3 460 [eV]**
TS-1-100	98.99	1.08	46.9	37	15	48
TS-1-25	44.34	2.41	24.3	5	58	37
ETS-10	11.49	9.60	3.6	--	100	--

3.2. Membrane Characterization

3.2.1. TGA

TGA curves for the different sets of MMMs can be seen in Fig. 5. Thermal gravimetric analyses show an increase of the thermal stability as the inorganic loading increases. The first loss of weight till 120 °C is due to the moisture evaporation of samples. The weight losses corresponding to the moisture evaporation range between 0.5 – 2 wt.% lost. These losses are higher in the unfilled membrane than in the MMMs due to the hydrophobicity of the fillers [48]. The following pronounced weight reduction between 150 °C and 300 °C is related to the evaporation of rests of solvent (T_{boil} (NMP)= 204.3 °C). The NMP residue ranges from 3 wt.% to 6 wt.% for MMMs, however unfilled membranes shows a higher

residue of NMP reaching the 9 wt.%. It indicates that the main part of the NMP residue is placed in the polymeric matrix instead of the pores of the particles. The increase of mobility of the polymer chains with the increment of the temperature, promotes a desorption of the NMP trapped between the polymer chains [49]. The decomposition temperature (T_d), calculated by the minimum of the first derivative, drops for MMMs compared to the unfilled Matrimid® membrane. Polyimide membrane shows a T_d of 526.2 °C and a weight loss of 22.3%, while the T_d of the MMMs ranges between 514.1 °C and 501.7 °C, and the weight loss varies between 20.3% and 12.4%. The slight decreases of T_d of MMMs can be due to the introduction of defects into the membrane. Overall, MMMs containing titanosilicates are able to stand sufficiently high temperatures to operate in different work conditions.

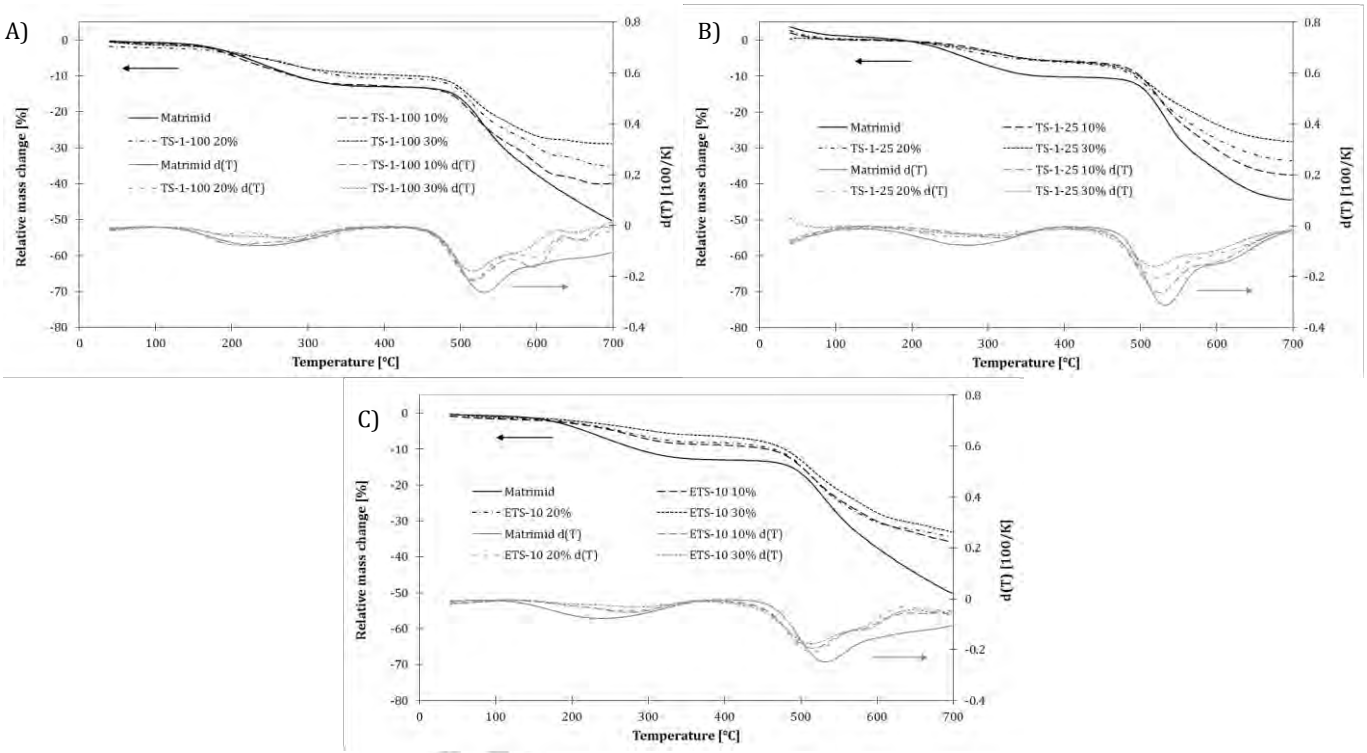

Fig. 5. TGA curves and their first derivatives for MMMs A) TS-1-100 B) TS-1-25 and C) ETS-10

3.2.2. DSC analyses

Glass transition temperatures of the different MMMs prepared in this work are listed in Table 2. The Matrimid® result is in agreement with literature [50]. DSC results show an increase of the T_g of the membrane with the increase of the inorganic loading because Matrimid® polymeric chains are able to penetrate into the microporous zeolites [51,52]. ETS-10 pores (7.6 × 4.9 Å) are wider than TS-1 pores (5.1 × 5.5 Å). Therefore, a larger penetration of polymer chains into the ETS-10 pores is expected. It causes a bigger constriction of the polymeric chains, reducing its possibilities to move, and increases the T_g. Difference between TS-1-100 and TS-1-25 can be due to a different structure of their surface. Moretti et al. [47] studied the different chemical states of Ti inside of microporous TS-1 with different Ti content. According to this work, during the synthesis of TS-1 with higher amount of Ti, a higher amount of segregated TiO_2 crystal (5 nm) undetectable by

XRD are deposited at the external surface of the TS-1 crystallite. The TiO_2 nanoparticles bring a better adhesion of the particles, increasing the rigidity of the polymeric chains.

Table 2. Glass transition temperatures of MMMs containing titanosilicate.

Sample	Zeolite (wt. %)	Polymer (wt. %)	T_g [°C][a]
Matrimid®	0	100	313.5
TS1-100-10%	10	90	315.5
TS1-100-20%	20	80	328.2
TS1-100-30%	30	70	331.7
TS1-25-10%	10	90	318.2
TS1-25-20%	20	80	324.4
TS1-25-30%	30	70	327.8
ETS-10-10%	10	90	315.2
ETS-10-20%	20	80	331.8
ETS-10-30%	30	70	336.4

[a] Typical error in DSC results varies from ±0.5 - 2 °C

3.2.3. SEM

In the Fig. 6 SEM micrographics of MMMs TS-1-25 cross-sections are presented, these MMMs also show a good compatibility between the polymer and the zeolites, and good filler dispersion. It is worthy to point that even being the same type of zeolites, at high magnification the TS-1-25 compared to TS-1-100 shows a better interface with a reduction of "sieve in a cage" morphology cases.

In Fig. 7A and B, SEM images of cross-sections of MMMs TS-1-100 with 20 wt.% loading can be observed, (rest of MMMs-TS-1-100 can be seen in Fig.S3 of ESI). In general terms, a good compatibility and dispersion between the polymeric matrix and the zeolite is achieved due to the mixing protocol. Although the interface between particle and polymer is sufficiently compatible, some of the particles present “a sieve in a cage" morphology in the higher magnification micrographics.

As it is shown on Fig. 7 C) and D) and Fig. S5 (ESI) the structure of MMMs containing ETS-10 is influenced by sedimentation of ETS-10 particles due to their size (610 nm) which is approximately 2.5 times bigger than in the case of TS-1-100. In this case, the mixing protocol is not appropriate for this particle size, and more volatile solvent must be used. However, the compatibility between the zeolites and the polymer is good to provide a membrane free of interfacial voids.

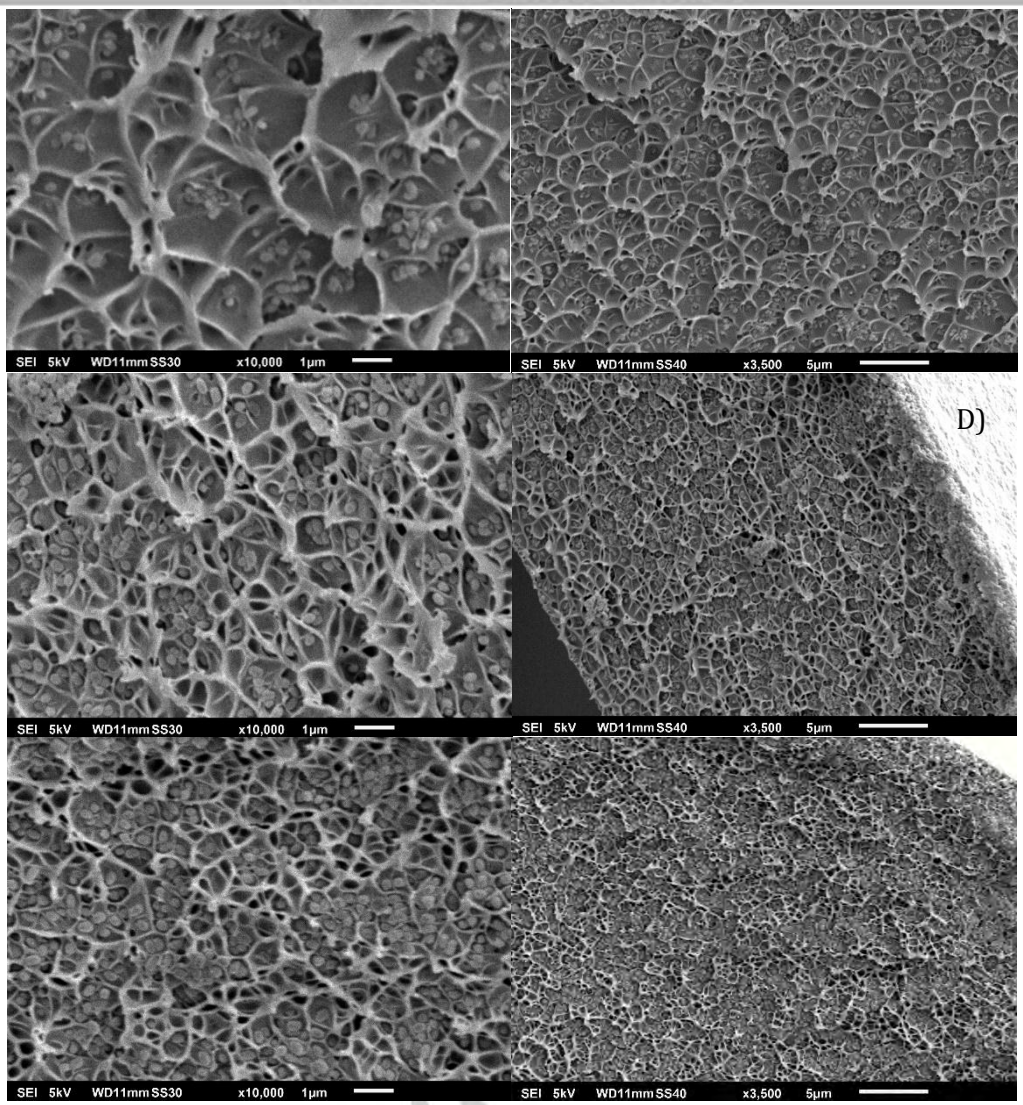

Fig. 6. SEM Images of MMM based on TS-1 (Si/Ti=25) at 10000X and 3500X respectively. A) and B) MMM loaded at 10 wt.%. C) and D) at 20 wt.%. and E) and F) 30 wt.%.

In all images, characteristic fracture morphology of MMMs can be observed. Concavities where the particles are placed in the center of them appear during the fracture. Moreover, higher the inorganic loading is, smaller the concavities that are produced. A reason for the formation of those cavities is a plastic deformation around the particles during the break. Inorganic particles introduce a concentration of internal stress around the particles. When the bending stress is applied, a fast fragile fracture is produced around the particles due to the concentration of stress, but the rest of the matrix breaks as ductile material [51]. On the other hand, the greater compatibility of TS-1-25 than TS-1-100 is most probably due to the higher amount of TiO_2 nanoparticles [47] at the surface which promote a better adhesion between particles and the carbonyl group from Matrimid®. It is in coherence with the XPS results explained previously which show a higher amount of TiO_2 on the surface of TS-1-25 than on the TS-1-100 surface.

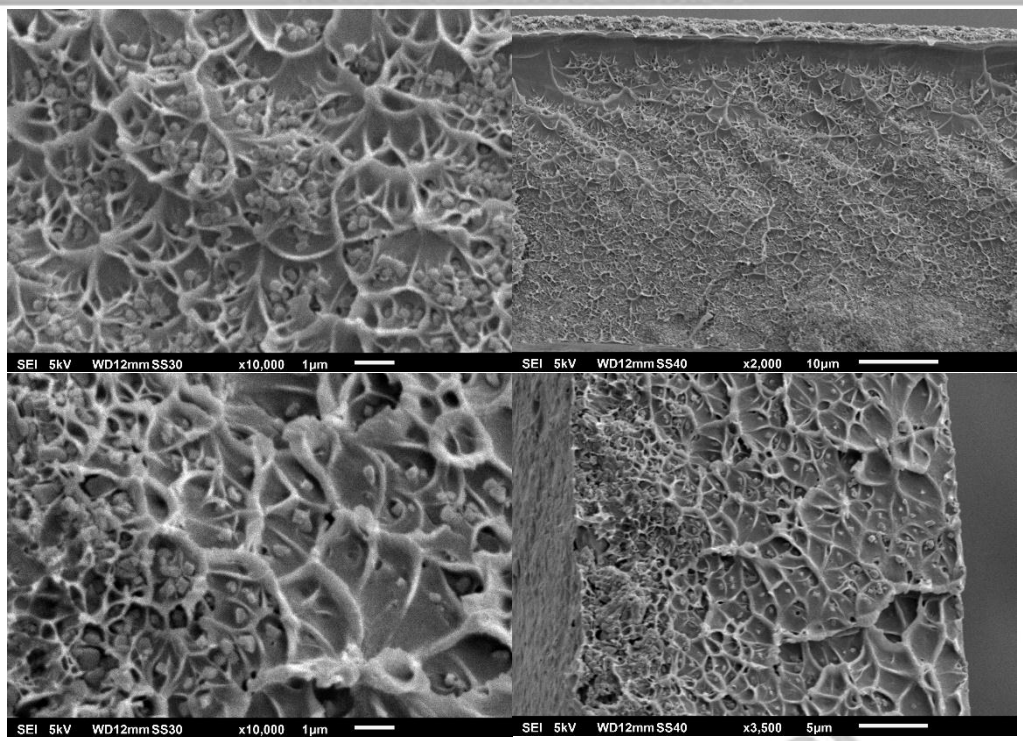

Fig. 7. SEM Images of MMM based on TS-100 with 20 wt.% loading at magnification of A) 10000X and B) 2000X and MMM using ETS-10 with 20 wt.% loading at magnification of C) 10000X and D) 3500X.

3.2.4. Gas separation

The incorporation of each titanosilicate leads to a different behavior of the MMMs due to the different adsorption behavior of the zeolites. The zeolites used have a pore diameter around 5 Å, the molecular sieving effect can be discarded for the separation of CO_2 and CH_4 with a kinetic diameter of 3.3 Å and 3.8 Å, respectively [37]. In Table 3, a summary of membrane performances is shown.

Table 3. Summary of permeabilities [Barrers] and separation factor of the different MMMs measured at ΔP=8bars, 35°C and 50/50 vol/vol CO_2/CH_4 feed composition.

Sample	Separation Factor	P_{CO_2} [Barrers]	P_{CH_4} [Barrers]
Matrimid®	25.5 ± 2.9	5.0 ± 0.3	0.20 ± 0.01
TS1-100-10%	26.8 ± 2.7	7.2 ± 0.9	0.27 ± 0.05
TS1-100-20%	26.3 ± 0.7	8.1 ± 1.1	0.31 ± 0.04
TS1-100-30%	25.0 ± 0.7	9.6 ± 1.3	0.45 ± 0.15
TS1-25-10%	31.5 ± 1.7	7.4 ± 0.2	0.24 ± 0.01
TS1-25-20%	31.6 ± 1.4	7.9 ± 1.4	0.25 ± 0.03
TS1-25-30%	30.8 ± 1.4	9.5 ± 1.2	0.31 ± 0.03
ETS-10-10%	32.6 ± 1.7	5.8 ± 0.5	0.18 ± 0.02
ETS-10-20%	33.3 ± 2.3	5.8 ± 0.5	0.18 ± 0.03
ETS-10-30%	27.5 ± 1.5	6.2 ± 0.3	0.23 ± 0.01

3.2.4.1. TS-1 (Si/Ti = 100) MMMs

In Fig. 8, graphs of absolute and normalized values of CO_2 and CH_4 permeabilities and separation factors are displayed. These membranes show an increment of 42.7%, 60.3% and 90.1% of normalized CO_2 permeabilities for 10 wt.%, 20 wt.% and 30 wt.% inorganic loading respectively. Regarding CH_4 permeabilities, a lower increase than for the CO_2 permeabilites is reached. MMMs of 10 wt.% and 20 wt.% of inorganic loading undergo an increment of 35.7% and 53.8% respectively. However, in the MMM-30 wt.% a significant increase of CH_4 permeability is obtained, reaching a value of 123.2% higher than the neat polyimide membrane. With respect to the separation factor, no significant increase is achieved. MMMs of 10 wt.% and 20 wt.% show a slight increase of separation factor, 5.3% and 3% respectively. MMMs with the highest inorganic content, presents a decrease of separation factor of 2%. This slight reduction comes as a result of the introduction of more defects such as voids around the particles and introduction of clusters due to the higher amount of inorganic filler in the membrane with the highest loading. Normalized CO_2 permeability shows a clear trend following a linear increase with the inorganic loading. In the case of normalized CH_4 permeability, the membrane using the 30 wt.% is clearly out of the trend. It can be explained by the introduction of clusters and voids, as it is observed in the SEM images (Fig. S5 E and F of ESI). Consequently, the normalized separation factor is almost constant, with an slight decrease for the highest loading.

The generally higher permeability for carbon dioxide than for methane is due to the better solubility of carbon dioxide. Addition of TS-1 leads to increase in both permeabilities. Different enhancement of permeabilities arises from the internal hydroxyl groups nests of TS-1 [29] that promote the polarization of CO_2. This electrostatic interaction between the quadrupole moment of carbon dioxide and the surface functional groups enhances the adsorption of this gas [53]. Methane is not a polarizable molecule, thus, increase of CH_4 permeability is mainly due to the improvement of the diffusivity of methane through the inorganic zeolites. In case of MMM-30 wt.%, the abrupt increase is because the introduction of a higher amount of defects (voids, clusters, “sieve in a cage morphologies” e.g.). An only slight improvement in separation factor is because permeabilities of both gases increase quasi in the same rate.

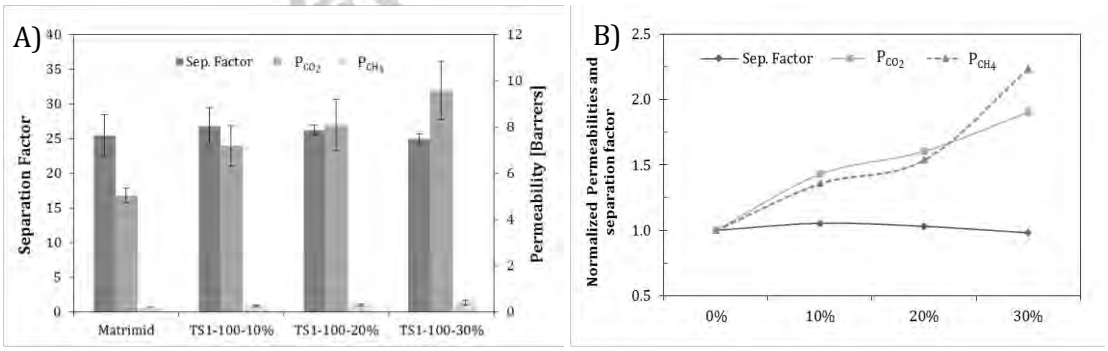

Fig. 8. Mixed gas permeabilities and separation factor of MMMs containing TS-1-100 measured at 35°C and ΔP = 8bars A) absolute values, B) normalized.

3.2.4.2. TS-1 (Si/Ti = 25) MMMs

In the case of MMMs using TS-1-25, Fig. 9, a different behavior than for TS-1-100 is observed. These MMMs present not only an increase of permeability but also an increment of selectivity. Regarding CO_2 permeability, a continuous increment of performance is achieved. A permeability growth of 46.2%, 56.1% and 89.1% is accomplished for MMMs of 10 wt.%, 20 wt.%, and 30 wt.% respectively. Concerning CH_4 permeability, increments are more reduced compared to MMMs TS-1-100. CH_4 permeability only experiences an enlargement of 17.5%, 24.5% and 54.6% with the increment of zeolite content. The larger differences in the increment of permeabilities cause the increase of separation factor around 20% for all the samples. Normalized permeabilities (CO_2 and CH_4) show a linear increment with the increase of the inorganic loading. Normalized separation factor shows a step increment respect to the unfilled membrane independently of the inorganic loading for all the MMMs.

When the content of Ti is higher, the number of linkages Si-O-Ti, which are more acidic than Si-O-Si, also increases. Therefore, when there is more Ti incorporated to the silica matrix; the sorption capacity increases. Furthermore, the incorporation of the larger sized Ti (IV) species replacing Si (IV) increases the unit cell volume, hence the volume-filling phenomenon is also contributing to increase of CO_2 sorption [49]. Methane permeability does not show the same increment as carbon dioxide because the polar molecules are adsorbed in the metal centers avoiding the sorption of apolar molecules [54]. As a result, the separation factor increases. Moreover, the presence of the TiO_2 nanoparticles on the surface of the TS-1-25 particles promotes a better adhesion between the particles and the polymeric matrix. It avoids the creation of defects such as “sieve in a cage” morphologies and it improves the separation performance of the membranes.

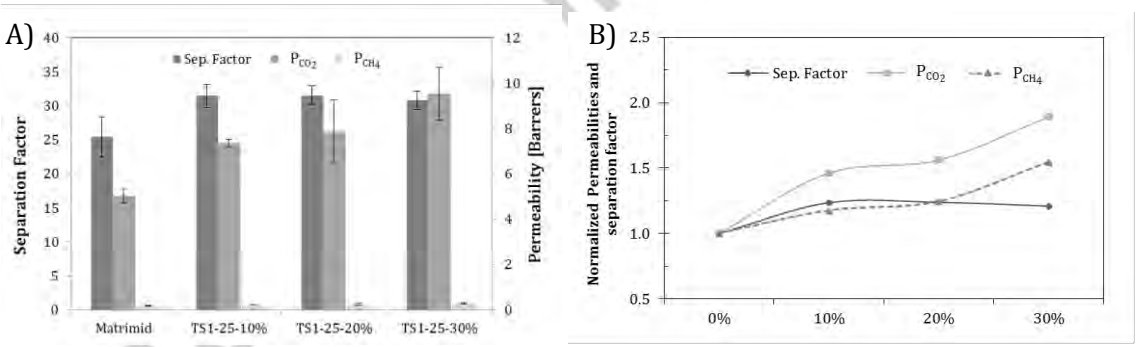

Fig. 9. Mixed gas permeabilities and separation factor of MMMs containing TS-1-25 measured at 35°C and ΔP = 8bars A) absolute values, B) normalized.

3.2.4.3. ETS-10 MMMs

MMMs containing ETS-10 achieve the highest augmentation in separation factor with respect to the unfilled polyimide membrane, increasing it as high as 30.8% for 20 wt.% ETS-10 MMM. For 10 wt.% MMM, the improvement achieved is 28.1%. However, for 30 wt.% MMM the increment of separation factor drops to 7.8% as a result of the introduction of defects (clusters, voids etc.) with the highest inorganic loading. Furthermore, for this 30 wt.% MMM an unexpected increment of both permeabilities is

observed (22.4% and 7.8% increment for CO_2 and CH_4 permeabilities respectively), confirming the creation of an important number of defects inside the membrane (Fig. S6 D and F of ESI). Regarding carbon dioxide permeability, a lower increase than for the other MMMs in this study is achieved. For 10 wt.% and 20 wt.% MMMs, CO_2 permeability arose 15.8% and 15.1% respectively. On the contrary, methane permeability remains almost constant for 10 wt.% and 20 wt.% MMMs showing a decrease of the 10% in both cases. Observing the normalized permeabilities, CO_2 permeability shows a constant value for the MMMs with a slight increment respect to the unfilled membrane. On the contrary, CH_4 permeability slightly decrease till 30 wt.% membrane when a sudden increment of both permeabilities coincides with the loss of selectivity. As it is explained previously, it is due to the imperfections observed in the SEM images.

The high exchange capacity and the cations presented (Na^+ and K^+) in the framework of ETS-10 promote the preferential adsorption of carbon dioxide against methane which entails a more improved separation factor than for the rest of MMMs studied in this work. The low increase of permeabilities is a consequence of the sedimentation of the zeolites inside the matrix. Moreover, ETS-10 has large pores (7.6 × 4.9 Å) which can be easily blocked by the intrusion of polymer chains. Decreasing of methane permeability can be due to rigidification of the polymer around the particle, increasing the tortuosity of the path and as a result, decreasing the permeability.

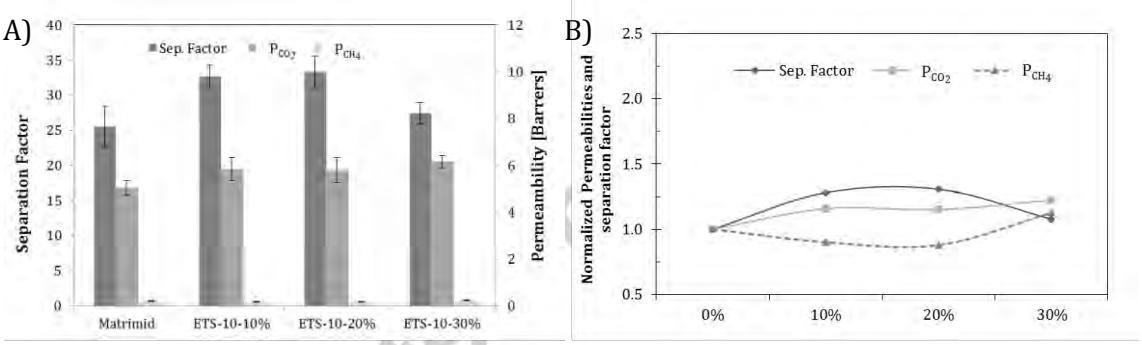

Fig. 10. Mixed gas permeabilities and separation factor of MMMs containing ETS-10 measured at 35°C and ΔP = 8bars A) absolute values, B) normalized.

Sorribas et al. [55] studied the introduction of different ETS-10 particles into a commercial polysulfone from Aldrich, the result obtained showed similar behavior as in this work. CO_2 permeability showed a slight increment of 1 Barrer with respect to the unfilled membranes, and the ideal selectivity showed an increment of 25%, as in this work also happens. Loloie et al. [56] studied the influence of addition of ZSM-5 (an aluminosilicate MFI zeolite) into Matrimid® by means of single gas measurements at 10 bar and 35 °C. These results are in agreement with the results reported in our work. ZSM-5 increased the permeability only 1.5 Barrers at the maximum inorganic load studied (7 wt.%), and ideal selectivity shows an increment with the inorganic load. Comparison of our system and other studies using layered titanosilicates (JDF-L1) [19] shows that the layered conformation of the zeolite besides its small pore size (3 Å) lead to an increment of the tortuosity of the path, decreasing the permeability and increasing the selectivity when the compatibility of the polymer is optimal, as it is the case for polyimides. However, the

addition of JDF-L1 to polyamide PA6 [57] does not show any significant effect on the composite material due to the low permeability of unfilled polyamide. Combination of a mesoporous silica (MCM-41) and a layered titanosilicate (JDF-L1) using 6FDA copolyimide was studied by Galve et al. [18] obtaining a combination of the different behaviors: an increment of selectivity due to the incorporation of the layered materials and an increment of the permeability due to the mesoporous materials. In our work, the results obtained for TS-1-25 and ETS-10 and increment of permselectivity is also achieved.

3.2.5. Mixed Matrix Membranes Model

Different models for MMMs have been proposed in order to determine the effect of the incorporation of a dispersed phase into the continuous phase. Different models attempt to describe the morphology of the resulting membranes including ideal and non-ideal configuration as well as estimate the final permselectivity properties of the composite material [58]. One of the most applied models for description of permeation trough the MMMs is Maxwell-Wagner-Sillar model. This model was developed in 1873 to predict the dielectric permittivity of heterogonous material. Due to the similarities between electric conductivity and the permeation of species through the MMMs [59], the permeability is expressed by the following equation [60].

Maxwell-Wagner-Sillar extended model:

$$P_{eff} = P_c \frac{nP_d+(1-n)P_c-(1-n)\varphi(P_c-P_d)}{nP_d+(1-n)P_c+n\varphi(P_c-P_d)} \quad \text{Eq. 8}$$

The n is the particle shape factor which can range between 0 and 1. At the limit of n = 0, the system is considered as a parallel two layers, where the permeability is the arithmetic mean of both materials. On the contrary, at the limit of n = 1, the system is considered as a series of two different materials layers [58]. For ideal morphologies with a good dispersion of spherical particles without an extra-phase (rigidification, voids) around the particles n is considered 1/3. Therefore, the extended Maxwell model equation can be expressed as the Eq. 9.

$$P_{eff} = P_c \frac{P_d+2P_c-2\varphi(P_c-P_d)}{P_d+2P_c+\varphi(P_c-P_d)} = P_c \frac{2(1-\varphi)+\alpha(1+2\varphi)}{(2+\varphi)+\alpha(1-\varphi)} \quad \text{Eq. 9}$$

$$\alpha = \frac{P_d}{P_c} \quad \text{Eq. 10}$$

In these equations P_{eff} corresponds to the effective permeability of the membrane, P_d to the permeability of dispersed phase (particles) and P_c to the permeability of continues phase (polymer), respectively. The φ is the particle volumetric loading calculated using Eq. 11 [61], where w_f and w_p are the weight of the filler and the polymer, respectively and ρ is the density either of the filler or polymer. The values of the densities for each phase were obtained from the literature. Densities of the MFI zeolite, ETS-10 and polymer are 1760 kg/m^3 [62], 1750 kg/m^3 [63] and 1220 kg/m^3 [49], respectively.

$$\varphi = \frac{w_f/\rho_f}{w_f/\rho_f + w_p/\rho_p} \quad \text{Eq. 11}$$

In order to calculate particle permeability, Langmuir constants q_{mi} and K_i (Eq. 12) were determined by means of processing CO_2 and CH_4 adsorption isotherms measured in pressure range from 0 to 9 atms using Micromeritics ASAP 2050 (Fig. S6 and Fig S7 of ESI).

$$q = \frac{q_{mi} K_i p}{1 + K_i p} \quad \text{Eq. 12}$$

The mass transfer in microporous material, especially in zeolites, is often referred to as configurational diffusion, which is characterized by its activated nature. The molecules can either retain a gaseous character in the micropores or they are adsorbed in the micropore surface [64]. The gas flux through microporous layer was calculated based on Eq. 13

$$J_i = \rho_s q_{mi} \frac{D_{i0}}{L} \frac{\ln(1 + K_i p_i^F)}{\ln(1 + K_i p_i^P)} \quad \text{Eq. 13}$$

where L is thickness of the layer, ρ_s the density of the layer (dispersed phase), D_{0i} the corrected diffusion coefficient and p_i is the partial pressure of the component i in the feed or in the permeate side, respectively. As far as our knowledge, there is a lack of consistent experimental data and values of corrected diffusivities of CO_2 and CH_4 in TS-1 neither ETS-10. For this reason, the Knudsen diffusion coefficient is assumed as D_{0i} (Eq. 14) for estimation of permeabilities of dispersed phase, as proposed in literature [65].

$$D_{0i} = \frac{2r}{3} \sqrt{\frac{8RT}{\pi M_i}} \quad \text{Eq. 14}$$

The r in Eq. 14 introduces the pore radius; M is the gas molecular weight and T the temperature. The Langmuir coefficients q_{mi} and K_i, together with calculated D_{i0} are disclosed in the Table 4. Particle permeability is calculated using Eq. 15. As the pressure in the permeate side is very low compared to the feed side, it can be neglected and the Eq. 15 can be simplified to the final Eq. 16.

$$P_d = \frac{J_i L}{(p_i^F - p_i^P)} = \frac{D_{0i} q_{mi} \rho_s}{(p_i^F - p_i^P)} \frac{\ln(1 + K_i p_i^F)}{\ln(1 + K_i p_i^P)} \quad \text{Eq. 15}$$

$$P_d = \frac{D_{0i} q_{mi} \rho_s}{p_i^F} \ln(1 + K_i p_i^F) \quad \text{Eq. 16}$$

In order to evaluate the deviation of predicted values from experimental data, the relative error (RE) was calculated using Eq. 17 [65].

$$\%RE_i = \frac{P_i^{cal} - P_i^{exp}}{P_i^{exp}} \cdot 100 \quad \text{Eq. 17}$$

Table 4. Calculated Langmuir Parameters.

Particle	Gas	Langmuir Parameters		Knudsen
		q_{mi} [mmol/g]	K_i[1/atm]	D_{0i} [m²/s]
TS-1-100	CO_2	4.46	0.46	$1.76 \cdot 10^{-7}$
	CH_4	2.21	0.31	$2.32 \cdot 10^{-7}$
TS-1-25	CO_2	4.77	0.45	$1.76 \cdot 10^{-7}$
	CH_4	2.11	0.31	$2.32 \cdot 10^{-7}$
ETS-10	CO_2	1.78	1.25	$2.43 \cdot 10^{-7}$
	CH_4	0.81	0.43	$3.21 \cdot 10^{-7}$

As it can be observed in the q_{mi} values for the different TS-1 particles, TS-1-25 shows a slightly higher adsorption for CO_2 and lower for CH_4 than TS-1-100. These results are in agreement with the results obtained from the evaluation of gas performance. However, the minor difference of the q_{mi} for the TS-1 samples compared with the differences in the gas separation performance can be explained because of the filling pore effect of the zeolite.

Table 5. Comparison of experimental data and data obtained from Maxwell model and their error deviation.

Membrane	Experimental Data		Maxwell Model Data		CO_2 Error	CH_4 Error
	P_{CO_2} [Barrer]	P_{CH_4} [Barrer]	P_{CO_2} [Barrer]	P_{CH_4} [Barrer]	%RE	%RE
TS-1-100-10%	7.2	0.27	6.2	0.25	-13.5	-8.6
TS-1-100-20%	8.1	0.31	7.7	0.31	-4.9	-1.6
TS-1-100-30%	9.6	0.45	9.6	0.38	0.0	-15.5
TS-1-25-10%	7.4	0.24	6.2	0.25	-15.7	2.8
TS-1-25-20%	7.9	0.25	7.7	0.31	-2.3	22.0
TS-1-25-30%	9.5	0.31	9.6	0.38	0.5	22.6
ETS-10-10%	5.8	0.18	6.2	0.25	6.6	37.2
ETS-10-20%	5.8	0.18	7.7	0.31	32.8	69.8
ETS-10-30%	6.2	0.23	9.6	0.38	55.6	65.7

Calculated permeabilities from Maxwell model are presented in Table 5. Predicted CO_2 permeability values for membranes filled with TS-1-100 particles are in good agreement with obtained experimental data, showing only a slight underestimation in range of relative error between 5 to 15%. With increasing content of filler the relative error is decreasing. CH_4 permeabilities for TS-1-100 MMMs show similar underestimation but with opposite trend (the relative error is increasing with higher content of filler). In the case of TS-1-25 MMMs, CO_2 permeabilities also show a good agreement with the experimental data, however CH_4 permeabilities are overestimated by the Maxwell model. The relative error in this case is slightly higher. It can be explained by the same reasons exposed above. Additionally, the calculated data are not accounting for the competitive adsorption of CO_2 and CH_4. The biggest disagreement show calculated data for ETS-10, it can be due to the sedimentation of the particles in these membranes. Maxwell model assumes an ideal morphology between both phases with homogenous dispersion of the dispersed phase. Moreover, this model assumes spherical particles. Although TS-1 particles show an ellipsoid shape which can be easier applied to this model, ETS-10 particles are trucked pyramidal shape. This issue can introduce some error in the estimation of the modelled data. Moreover, sedimentation of ETS-10 particles is the other reason of the important differences between experimental data and calculated permeabilities. If ETS-10 MMMs are considered as a two layers in series configuration, the theoretical permeabilities can be calculated using Eq. 8 and $n = 1$. These results are presented in Table 6.

Table 6. Comparison between calculated permeability of ETS-10 MMMs using extended Maxwell model (n = 1) and experimental data and their error deviation.

Membrane	Experimental Data		Maxwell Model Data		CO_2 Error	CH_4 Error
	P_{CO_2} [Barrer]	P_{CH_4} [Barrer]	P_{CO_2} [Barrer]	P_{CH_4} [Barrer]	%RE	%RE
ETS-10-10%	5.8	0.18	5.4	0.22	7.0	-19.7
ETS-10-20%	5.8	0.18	5.9	0.23	-2.0	-30.5
ETS-10-30%	6.2	0.23	6.5	0.26	-6.1	-12.9

An important reduction on the error is observed, obtaining very close results for CO_2 permeabilities. It means that the main source of the error corresponds to morphological characteristics of the membrane such as: dispersion of filler (sedimentation, clusters etc.),

or introduction of a third phase between dispersed and continuous phase ("sieve in a cage" morphologies, rigidified polymer around the particles).

A comparison of relative errors showed in Table 5 and Table 6 for ETS-10 MMMs discloses a maximum error reduction up to 49.5% for CO_2 permeability and 52.8% for CH_4 permeability for ETS-10-30% membrane. In the case of ETS-10-20% membrane, the reduction is the 30.8% for CO_2 permeability and 39.3% for CH_4 permeability. Only in the case of ETS-10-10% membrane the error increases a 0.4% for CO_2 permeability, but a reduction of the error is showed in CH_4 permeability of 17.5%. It can be concluded that the two layers material in series model leads the errors for ETS-10 MMMs in more acceptable ranges than using the Maxwell model when n = 1/3. Furthermore, this approach is in agreement with the morphology showed in the SEM micrographies.

In addition to Maxwell model, other models have been developed [58]. The Lewis-Nielsen (Eq. 18 and Eq. 19) model was developed initially for elastic modulus of composite materials where ϕ_m is the maximum packing volume fraction of the filler particles and usually its value is considered to be 0.64 for a random close packing of uniform spheres. ϕ_m expresses the relation with the particle size distribution, particle shape and aggregation of particles.

$$\frac{P_{eff}}{P_c} = \frac{1+2\varphi(\alpha-1)/(\alpha+2)}{1-\psi\varphi(\alpha-1)/(\alpha+2)} \qquad \text{Eq. 18}$$

$$\psi = 1 + \left(\frac{1-\phi_m}{\phi_m^2}\right)\varphi \qquad \text{Eq. 19}$$

Carbon dioxide and methane permeabilities were calculated using this model in order to check if it can express better than Maxwell model the behavior of the MMMs produced in this work. In the Table 7 the calculated permeabilities values as well as the relative error can be observed for comparison.

Table 7. Comparison of experimental data and data obtained from Lewis-Nielsen model and their error deviation.

Membrane	Experimental Data		Lewis-Nielsen Model Data		CO_2 Error	CH_4 Error
	P_{CO_2} [Barrer]	P_{CH_4} [Barrer]	P_{CO_2} [Barrer]	P_{CH_4} [Barrer]	%RE	%RE
TS-1-100-10%	7.2	0.27	6.2	0.25	-13.3	-8.4
TS-1-100-20%	8.1	0.31	7.8	0.31	-3.2	0.2
TS-1-100-30%	9.6	0.45	10.1	0.40	5.4	-11.0
TS-1-25-10%	7.4	0.24	6.2	0.25	-15.5	3.0
TS-1-25-20%	7.9	0.25	7.8	0.31	-1.0	23.7
TS-1-25-30%	9.5	0.31	10.0	0.40	4.8	27.9
ETS-10-10%	5.8	0.18	6.2	0.25	6.2	36.7
ETS-10-20%	5.8	0.18	7.6	0.30	31.5	68.1
ETS-10-30%	6.2	0.23	9.4	0.37	52.3	62.1

Lewis-Nielsen model is able to predict the experimental values for carbon dioxide permeability of TS-1 MMMs with an acceptable range of error. In the case of methane permeability, relative errors arise up to 27.9%. However, ETS-10 MMMs calculated values highly differ from the experimental ones. It can be due to the sedimentation of the particles and the assumption of spherical shape particles. The relative errors of Maxwell

and Lewis-Nielsen models are in the same range, showing than the dispersion of the fillers plays an important role in the prediction of the models.

Conclusions

Three titanosilicate (TS-1-100, TS-1-25 and ETS-10) nanoparticles were synthesized and flat dense MMMs with significant inorganic loadings (10, 20 and 30 wt.%) were manufactured from these nanoparticles using Matrimid® as the matrix. Good dispersions were achieved for TS-1 nanoparticles. Whereas ETS-10 nanoparticles, even though ETS-10 particles synthesized in this work (610 ± 67 nm) are in the range of the particle size reported in literature, were more settled during membrane preparation due to its bigger particle size compared with TS-1 particles. In terms of compatibility, TS-1-25 and ETS-10 particles showed a continuous interface with the polymeric matrix in SEM high-magnification images, while TS-1-100 showed some "sieve in a cage" morphologies. MMMs were tested at 50/50 vol./vol. CO_2/CH_4 feed composition, 35 °C and ΔP = 8bars. The gas separation results in the case of TS-1 MMMs revealed different behavior of these membranes. MMMs using TS-1-25 as filler showed a maximum increase of 89.1% of CO_2 permeability for the MMM with 30 wt.% of filler and 23.9% increase in separation factor for 20 wt.% MMM. In the case of TS-1-100 only permeability increased significantly with a maximum increase of 90.1% in the case of 30 wt.% loading. These results showed that content of Ti inside TS-1 plays an important role in the gas separation performance, facilitating the permeability of carbon dioxide due to a different sorption capacity. High content of Ti inside the zeolite lead to increase CO_2 adsorption. As a result, a high separation factor is achieved. Regarding ETS-10 MMMs, both permeability and separation factor increased slightly with respect to the unfilled membranes, due to the deposition of the zeolite at the bottom of the membrane. Therefore, ETS-10 zeolites are not an appropriated filler using the preparation protocol established here. A high volatile solvent should be used in case of using ETS-10 like inorganic filler. In conclusion, it can be said that TS-1 (Si/Ti=25) is the most suitable filler to use in MMMs for gas separation applications.

Acknowledgments

The financial support of The Education, Audiovisual and Culture Executive Agency – EACEA/European Commission within the "Erasmus Mundus Doctorate in Membrane Engineering – EUDIME" (ERASMUS MUNDUS Programme 2009-2013, FPA n. 2011-0014, SGA n. 2012-1719) and the financial support of the Czech Science Foundation (grant GACR No. 15-06479S) are kindly acknowledged. We are also grateful to KU Leuven for support in the frame of OT (11/ 061), the Flemish Government for the Methusalem (CASAS) and FWO (G.0698.11) grants, and the Federal Government for an IAP grant (FS2).

References

[1] www.eia.gov, International Energy Statistics - EIA, (n.d.).

[2] Y. Xiao, B.T. Low, S.S. Hosseini, T.S. Chung, D.R. Paul, The strategies of molecular architecture and modification of polyimide-based membranes for CO2 removal from natural gas—A review, Prog. Polym. Sci. 34 (2009) 561–580.

[3] T.-S. Chung, L.Y. Jiang, Y. Li, S. Kulprathipanja, Mixed matrix membranes (MMMs) comprising organic polymers with dispersed inorganic fillers for gas separation, Prog. Polym. Sci. 32 (2007) 483–507.

[4] R.W. Baker, Future Directions of Membrane Gas Separation Technology, Ind. Eng. Chem. Res. 41 (2002) 1393–1411.

[5] P.S. Goh, a. F. Ismail, S.M. Sanip, B.C. Ng, M. Aziz, Recent advances of inorganic fillers in mixed matrix membrane for gas separation, Sep. Purif. Technol. 81 (2011) 243–264.

[6] Y. Zhang, J. Sunarso, S. Liu, R. Wang, Current status and development of membranes for CO2/CH4 separation: A review, Int. J. Greenh. Gas Control. 12 (2013) 84–107.

[7] L.M. Robeson, Correlation of separation factor versus permeability for polymeric membranes, J. Memb. Sci. 62 (1991) 165–185.

[8] L.M. Robeson, The upper bound revisited, J. Memb. Sci. 320 (2008) 390–400.

[9] M. Rezakazemi, A. Ebadi Amooghin, M.M. Montazer-Rahmati, A.F. Ismail, T. Matsuura, State-of-the-art membrane based CO2 separation using mixed matrix membranes (MMMs): An overview on current status and future directions, Prog. Polym. Sci. 39 (2014) 817–861.

[10] a. F. Ismail, P.S. Goh, S.M. Sanip, M. Aziz, Transport and separation properties of carbon nanotube-mixed matrix membrane, Sep. Purif. Technol. 70 (2009) 12–26.

[11] R.D. Noble, Perspectives on mixed matrix membranes, J. Memb. Sci. 378 (2011) 393–397.

[12] D. Bastani, N. Esmaeili, M. Asadollahi, Polymeric mixed matrix membranes containing zeolites as a filler for gas separation applications: A review, J. Ind. Eng. Chem. 19 (2013) 375–393.

[13] P. Burmann, B. Zornoza, C. Téllez, J. Coronas, Mixed matrix membranes comprising MOFs and porous silicate fillers prepared via spin coating for gas separation, Chem. Eng. Sci. 107 (2014) 66–75.

[14] B. Zornoza, O. Esekhile, W.J. Koros, C. Téllez, J. Coronas, Hollow silicalite-1 sphere-polymer mixed matrix membranes for gas separation, Sep. Purif. Technol. 77 (2011) 137–145.

[15] B. Zornoza, C. Téllez, J. Coronas, Mixed matrix membranes comprising glassy polymers and dispersed mesoporous silica spheres for gas separation, J. Memb. Sci. 368 (2011) 100–109.

[16] T. Suzuki, Y. Yamada, Characterization of 6FDA-based hyperbranched and linear polyimide-silica hybrid membranes by gas permeation and129Xe NMR measurements, J. Polym. Sci. Part B Polym. Phys. 44 (2006) 291–298.

[17] A.B. Beltran, G.M. Nisola, E. Cho, E.E.D. Lee, W.-J. Chung, Organosilane modified silica/polydimethylsiloxane mixed matrix membranes for enhanced propylene/nitrogen separation, Appl. Surf. Sci. 258 (2011) 337–345.

[18] A. Galve, D. Sieffert, C. Staudt, M. Ferrando, C. Güell, C. Téllez, et al., Combination of ordered mesoporous silica MCM-41 and layered titanosilicate JDF-L1 fillers for 6FDA-based copolyimide mixed matrix membranes, J. Memb. Sci. 431 (2013) 163–170.

[19] A. Galve, D. Sieffert, E. Vispe, C. Téllez, J. Coronas, C. Staudt, Copolyimide mixed matrix membranes with oriented microporous titanosilicate JDF-L1 sheet particles, J. Memb. Sci. 370 (2011) 131–140.

[20] a. Bos, I.G.M. Pünt, M. Wessling, H. Strathmann, Plasticization-resistant glassy polyimide membranes for CO2/CO4 separations, Sep. Purif. Technol. 14 (1998) 27–39.

[21] J.D. Wind, D.R. Paul, W.J. Koros, Natural gas permeation in polyimide membranes, J. Memb. Sci. 228 (2004) 227–236.

[22] S. Galioğlu, M.N. Ismail, J. Warzywoda, A. Sacco Jr, B. Akata, Preparation and microstructural characterization of oriented titanosilicate ETS-10 thin films on indium tin oxide surfaces, Microporous Mesoporous Mater. 131 (2010) 401–406.

[23] Z. Lin, Synthesis and characterisation of titanosilicate ETS-10 membranes, Microporous Mesoporous Mater. 67 (2004) 79–86.

[24] G. Peregot, G. Bellussi, C. Corno, M. Taramasso, F. Buonomot, A. Esposito, New Developments in Zeolite Science and Technology, Proceedings of the 7th International Zeolite Conference, Elsevier, 1986.

[25] H. van Bekkum, J.C. Jacobs, P.A., Flanigen, E.M., Jansen, Introduction to Zeolite Science and Practice, Elsevier B.V., 2001.

[26] G. Artioli, C. Lamberti, G.L. Marra, Neutron powder diffraction study of orthorhombic and monoclinic defective silicalite, Acta Crystallogr. Sect. B Struct. Sci. 56 (2000) 2–10.

[27] ENI, Titanium Silicalite (TS-1) zeolite based - Proprietary Catalyst, (2009).

[28] S.P. Mirajkar, A. Thangaraj, V.P. Shiralkar, Sorption properties of titanium silicate molecular sieves, J. Phys. Chem. 96 (1992) 3073–3079.

[29] F. Langerame, A.M. Salvi, M. Silletti, G. Moretti, XPS characterization of a synthetic Ti-containing MFI zeolite framework: The titanosilicalites, TS-1, Surf. Interface Anal. 40 (2008) 695–699.

[30] S.M. Kuznicki, Large-pored crystalline titanium molecular sieve zeolites, US Patent No. 4853202, 1989.

[31] M.W. Anderson, O. Terasaki, T. Ohsuna, A. Philippou, S.P. MacKay, A. Ferreira, et al., Structure of the microporous titanosilicate ETS-10, Nature. 367 (1994) 347–351.

[32] MFI Structure (IZA Database), Http://www.iza-Structure.org/databases/. (n.d.).

[33] I. Tiscornia, S. Irusta, C. Tellez, J. Coronas, J. Santamaria, Separation of propylene/propane mixtures by titanosilicate ETS-10 membranes prepared in one-step seeded hydrothermal synthesis, J. Memb. Sci. 311 (2008) 326–335.

[34] C. Casado, Z. Amghouz, J.R. García, K. Boulahya, J.M. González-Calbet, C. Téllez, et al., Synthesis and characterization of microporous titanosilicate ETS-10 obtained with different Ti sources, Mater. Res. Bull. 44 (2009) 1225–1231.

[35] I. Tiscornia, I. Kumakiri, R. Bredesen, C. Téllez, J. Coronas, Microporous titanosilicate ETS-10 membrane for high pressure CO2 separation, Sep. Purif. Technol. 73 (2010) 8–12.

[36] A. Anson, C.C.H. Lin, S.M. Kuznicki, J.A. Sawada, Adsorption of carbon dioxide, ethane, and methane on titanosilicate type molecular sieves, Chem. Eng. Sci. 64 (2009) 3683–3687.

[37] Q. Song, S.K. Nataraj, M. V. Roussenova, J.C. Tan, D.J. Hughes, W. Li, et al., Zeolitic imidazolate framework (ZIF-8) based polymer nanocomposite membranes for gas separation, Energy Environ. Sci. 5 (2012) 8359.

[38] D. a. Peru, R.J. Collins, Comparison of cold digestion methods for elemental analysis of a Y-type zeolite by inductively coupled plasma (ICP) spectrometry, Fresenius. J. Anal. Chem. 346 (1993) 909–913.

[39] A.L. Khan, S. Basu, A. Cano-Odena, I.F.J. Vankelecom, Novel high throughput equipment for membrane-based gas separations, J. Memb. Sci. 354 (2010) 32–39.

[40] R. Swaidan, X. Ma, E. Litwiller, I. Pinnau, High pressure pure- and mixed-gas separation of CO2/CH4 by thermally-rearranged and carbon molecular sieve membranes derived from a polyimide of intrinsic microporosity, J. Memb. Sci. 447 (2013) 387–394.

[41] F. Qiu, X. Wang, X. Zhang, H. Liu, S. Liu, K.L. Yeung, Preparation and properties of TS-1 zeolite and film using Sil-1 nanoparticles as seeds, Chem. Eng. J. 147 (2009) 316–322.

[42] D.T. Cong, Preparation and Characterization Of Composite Membranes With Microporous Separation Layer Based On Molecular Sieves, Institute of Chemical Technology Prague, 2012.

[43] N.A. Turta, M. Veltri, D. Vuono, P. De Luca, N. Bilba, A. Nastro, Effect of crystallization temperature on the synthesis of ETS-4 and ETS-10 titanosilicates, J. Porous Mater. 16 (2009) 527–536.

[44] M. V Shankar, J. Ye, Inorganic alkaline-sols as precursors for rapid synthesis of ETS-10 microporous titanosilicates and their photocatalytic reforming of methanol under visible-light irradiation, Catal. Commun. 11 (2009) 261–265.

[45] L. Lv, F. Su, X.S. Zhao, A reinforced study on the synthesis of microporous titanosilicate ETS-10, Microporous Mesoporous Mater. 76 (2004) 113–122.

[46] B.M. Faroldi, E. a Lombardo, L.M. Cornaglia, S. Irusta, Application of ETS-10 microporous titanosilicate as support of Ru nanoparticles for hydrogen production, Appl. Catal. A Gen. 417-418 (2012) 43–52.

[47] G. Moretti, a. M. Salvi, M.R. Guascito, F. Langerame, An XPS study of microporous and mesoporous titanosilicates, Surf. Interface Anal. 36 (2004) 1402–1412.

[48] D.P. Serrano, G. Calleja, J.A. Botas, F.J. Gutierrez, Characterization of adsorptive and hydrophobic properties of silicalite-1, ZSM-5, TS-1 and Beta zeolites by TPD techniques, Sep. Purif. Technol. 54 (2007) 1–9.

[49] S. Shahid, K. Nijmeijer, High pressure gas separation performance of mixed-matrix polymer membranes containing mesoporous Fe(BTC), J. Memb. Sci. 459 (2014) 33–44.

[50] a. Bos, I.G.M. Pünt, M. Wessling, H. Strathmann, CO2-induced plasticization phenomena in glassy polymers, J. Memb. Sci. 155 (1999) 67–78.

[51] Y. Zhang, K.J. Balkus, I.H. Musselman, J.P. Ferraris, Mixed-matrix membranes composed of Matrimid® and mesoporous ZSM-5 nanoparticles, J. Memb. Sci. 325 (2008) 28–39.

[52] I.F.J. Vankelecom, E. Merckx, M. Luts, J.B. Uytterhoeven, Incorporation of zeolites in polyimide membranes, J. Phys. Chem. 99 (1995) 13187–13192.

[53] K. Sumida, D.L. Rogow, J.A. Mason, T.M. McDonald, E.D. Bloch, Z.R. Herm, et al., Carbon dioxide capture in metal-organic frameworks., Chem. Rev. 112 (2012) 724–81.

[54] M.G. Clerici, The activity of titanium silicalite-1 (TS-1): Some considerations on its origin, Kinet. Catal. 56 (2015) 450–455.

[55] S. Sorribas, B. Comesaña-Gándara, A.E. Lozano, B. Zornoza, C. Téllez, J. Coronas, Insight into ETS-10 synthesis for the preparation of mixed matrix membranes for CO 2 /CH 4 gas separation, RSC Adv. 5 (2015) 102392–102398.

[56] M. Loloei, M. Omidkhah, A. Moghadassi, A.E. Amooghin, Preparation and characterization of Matrimid® 5218 based binary and ternary mixed matrix membranes for CO2 separation, Int. J. Greenh. Gas Control. 39 (2015) 225–235.

[57] C. Rubio, E. Piera, M.Á. Caballero, C. Téllez, J. Coronas, Synthesis of layered titanosilicate JDF-L1 for fabrication of composite polyamide 6 film, Appl. Clay Sci. 118 (2015) 151–157.

[58] H. Vinh-Thang, S. Kaliaguine, Predictive models for mixed-matrix membrane performance: A review, Chem. Rev. 113 (2013) 4980–5028.

[59] O. Bakhtiari, N. Sadeghi, Mixed matrix membranes' gas separation performance prediction using an analytical model, Chem. Eng. Res. Des. 93 (2015) 710–719.

[60] M. a. Aroon, a. F. Ismail, T. Matsuura, M.M. Montazer-Rahmati, Performance studies of mixed matrix membranes for gas separation: A review, Sep. Purif. Technol. 75 (2010) 229–242.

[61] S. Basu, A. Cano-Odena, I.F.J. Vankelecom, Asymmetric Matrimid??/[Cu3(BTC)2] mixed-matrix membranes for gas separations, J. Memb. Sci. 362 (2010) 478–487.

[62] M. Yu, J.L. Falconer, R.D. Noble, Adsorption of liquid mixtures on silicalite-1 zeolite: a density-bottle method., Langmuir. 21 (2005) 7390–7.

[63] Z. Ji, J. Warzywoda, A. Sacco, Titanosilicate ETS-10 thin film preparation on fused silica optical fibers, Microporous Mesoporous Mater. 101 (2007) 279–287.

[64] a. J. Burggraaf, Single gas permeation of thin zeolite (MFI) membranes: Theory and analysis of experimental observations, J. Memb. Sci. 155 (1999) 45–65.

[65] S.A. Hashemifard, A.F. Ismail, T. Matsuura, Prediction of gas permeability in mixed matrix membranes using theoretical models, J. Memb. Sci. 347 (2010) 53–61.

Highlights

- Titanosilicate (TS-1, ETS-10) were used as filler in MMMs for application in CO_2/CH_4 gas separation.
- Titanosilicates were synthesized in nanoparticle ranges from 260 nm to 610 nm.
- The content of Ti inside TS-1 plays an important role on separation factor.
- The content of titanosilicate in MMMs (0 – 30 wt%) showed an improvement not only on the permeation properties but also on the separation factor.